Lattice Poisson-Boltzmann Simulations of Electro-osmotic Flows in Microchannels

Jinku Wang[a)], Moran Wang[1,b)], Zhixin Li [a)]

[a)] *School of Aerospace, Tsinghua University, Beijing 100084, P.R. China*
[b)] *Department of Mechanical Engineering, The Johns Hopkins University, Baltimore, MD, 21218, USA*

Abstract: This paper presents the numerical results of electro-osmotic flows in micro- and nano-fluidics using a Lattice Poisson-Boltzmann method (LPBM) which combines a potential evolution method on discrete lattices to solve the nonlinear Poisson equation (Lattice Poisson method) with a density evolution method on discrete lattices to solve the Boltzmann-BGK equation (Lattice Boltzmann method). In an electrically driven osmotic flow field, the flow velocity increases with both the external electrical field strength and the surface zeta potential for flows in a homogeneous channel. However, for a given electrical field strength and zeta potential, electrically driven flows have an optimal ionic concentration and an optimum width that maximize the flow velocity. For pressure-driven flows, the electro-viscosity effect increases with the surface zeta potential, but has an ionic concentration that yields the largest electro-viscosity effect. The zeta potential arrangement has little effect on the electro-viscosity for heterogeneous channels. For flows driven by both an electrical force and a pressure gradient, various zeta potential arrangements were considered for maximize the mixing enhancement with a less energy dissipation.

Citation as: Jinku Wang, Moran Wang, and Zhixin Li. Lattice Poisson-Boltzmann Simulations of Electro-osmotic Flows in Microchannels. ***Journal of Colloid and Interface Science.*** **296**(2): 729-736, 2006

[1] Corresponding author. E-mail: moralwang@jhu.edu

1. Introduction

With the growing interest in bio-MEMS and bio-NEMS applications and fuel cell technologies, electrokinetic flows have become one of the most important non-mechanical techniques in micro- and nano-fluidics [1-4]. Electro-osmotic flows (EOF) have wide applications for pumping [5-8], separating [1,2] and mixing [9,10] in micro- and nano-scale devices. The electro-viscosity effect also increases the energy dissipation in the electrolyte solution transport [11,12].

Due to their many applications, numerical simulations of EOF in micro- and nano-channels have recently received a great amount of attention [13-20]. From the macroscopic point of view, the EOFs are governed by the Navier-Stokes equations for flow and the Poisson-Boltzmann equation for the electrical potential [13]. Some researchers have simulated EOF using these macroscopic equations [14,15]. In recent years, a mesoscopic statistics-based method, the lattice Boltzmann method (LBM), has been developed for EOF in micro-fluidic devices because external force fields can be more easily added to the lattice Boltzmann equation than to the Navier-Stokes equation [16-18, 21-25]. Recently, Guo et al.[25] divided the existing LBMs for the EOF into two categories based on the number components: single-fluid models and multi-fluid component models. The methods can also be divided into three categories based on main the solution methods for the electric potential as: conventional methods, the "moment propagation" method and the independent lattice Boltzmann method.

Most previous works used conventional numerical methods to solve the Poisson-Boltzmann equation, especially in its one dimensional linearized form [16-18]. The multigrid technique can greatly increase the efficiency of the iterative solution of the nonlinear Poisson-Boltzmann equation [21,26], but the technique can not easily be used to treat complex geometries. For charged suspensions, Warren [22] introduced the "moment propagation" method [27] to solve the electrical potential distribution. He and Li [23] proposed a different scheme for analyzing the electrochemical processes in an electrolyte by using an independent lattice Boltzmann method to solve the Poisson equation for the ion diffusion. However, this method was based on a locally electrically neutral assumption so it was not suitable for analyzing the dynamics of charged suspensions [24]. Recently, Guo et al. [25] developed He's method by directly solving the electric potential equation and investigated the Joule heating effect of electro-osmotic flow in microfluidic devices.

Following the spirit of He's method, this paper describes a consistent lattice evolution method which combines a lattice solution for the non-linear Poisson equation for the electrical potential with a lattice solution for the Bhatnagar-Gross-Krook (BGK) equation for incompressible fluid flows. Our method was independently developed, but similar with Guo's [25]. As with the standard LBM, this method can easily deal with complex boundary conditions and can be easily extended to 3D problems and parallel computing. The method was validated against an analytical solution and then used to simulate electro-osmotic flows in micro- and nano-scale channels. The pumping effect of electrically driven flows and the electro-viscosity effect in pressure driven flows were analyzed in both homogeneous and heterogeneous channels. The mixing enhancement in a heterogeneous channel with non-uniform surface zeta potential was also demonstrated.

2. Numerical method

2.1 Lattice Boltzmann method for fluids with external forces

The lattice Boltzmann method simulates transport phenomena by tracking the movements of molecule ensembles through the evolution of the distribution function [28]. The lattice Boltzmann equation can be derived from the Boltzmann equation [29]. For the flows with external forces, the continuous Boltzmann-BGK equation with an external force term, F, is

$$\frac{Df}{Dt} \equiv \partial_t f + (\boldsymbol{\xi} \cdot \nabla) f = -\frac{f - f^{eq}}{\tau_v} + F, \qquad (1)$$

where $f \equiv f(x, \boldsymbol{\xi}, t)$ is the single particle distribution function in the phase space $(x, \boldsymbol{\xi})$, $\boldsymbol{\xi}$ is the microscopic velocity, τ_v is the relaxation time, and f^{eq} is the Maxwell-Boltzmann equilibrium distribution. For a steady fluid immersed in a conservative force field, the equilibrium distribution function is defined by adding a Boltzmann factor to the Maxwell-Boltzmann distribution:

$$f^{eq} = \frac{\rho_0}{(2\pi RT)^{D/2}} \exp\left(-\frac{U}{kT}\right) \exp\left(-\frac{(\xi \mathbf{u} -)^2}{2RT}\right), \qquad (2)$$

where U is the potential energy of the conservative force field, ρ_0 is the fluid density where U is lowest, R is the ideal gas constant, D is the dimension of the calculation space(1D,2D or 3D), k is the Boltzmann constant, and $\mathbf{u}$ is the macroscopic velocity. Here the external force term, F, needs to be chosen carefully. Dimensional analysis led to the following form of F:

$$F = \frac{\mathbf{G}\xi(\mathbf{u} -)}{RT} f^{eq}, \qquad (3)$$

with $\mathbf{G}$ being the external force per unit mass [30]. Eq. (3) has a perfect accuracy (relative errors are totally less than 0.5% when comparing with analytical solutions for a Poisseuille flow), even though ones reported it was an only first order approximation [31].

The Chapman-Enskog expansion can be used to transform the Boltzmann-BGK equation, Eq. (1), into the correct continuum Navier-Stokes equations,

$$\rho \frac{\partial \mathbf{u}}{\partial t} + \rho \mathbf{u} \cdot \nabla \mathbf{u} = -\nabla P + \mu \nabla^2 \mathbf{u} + \mathbf{F}_E, \qquad (4)$$

where ρ is the solution density, P is the pressure, μ is the dynamic fluid viscosity and $\mathbf{F}_E$ is the electric force density vector. In general, the electrical body force in electrokinetic fluids can be expressed as:

$$\mathbf{F}_E = \mathbf{F}_{ext} + \rho_e(\mathbf{E}_{\text{int}} + \times_{\text{int}}) + _V, \qquad (5)$$

where $\mathbf{F}_{ext}$ represents the external field body forces, including the Lorentz force associated with any externally applied electric and magnetic field. For only an electrical field, $\mathbf{F}_{ext} = \rho_e \mathbf{E}$, where ρ_e is the net charge density and $\mathbf{E}$ is the electrical field strength. $\mathbf{E}_{\text{int}}$ and $\mathbf{B}_{\text{int}}$ are internally smoothed electrical and magnetic fields due to the motion of the charged particles inside the fluid. $\mathbf{F}_V$ is a single equivalent force density due to the intermolecular attraction [16].

For the two-dimensional case, third-order Gauss-Hermite quadrature leads to the nine-speed LBE model with the discrete velocities

$$e_\alpha = \begin{cases} (0,0) & \alpha = 0 \\ (\cos\theta_\alpha, \sin\theta_\alpha)c \quad \theta_\alpha = (\alpha - 1)\pi/2 & \alpha = 1,2,3,4 \\ \sqrt{2}(\cos\theta_\alpha, \sin\theta_\alpha)c \quad \theta_\alpha = (\alpha - 5)\pi/2 + \pi/4 & \alpha = 5,6,7,8 \end{cases}, \qquad (6)$$

where $c = \sqrt{3RT}$ and the equilibrium distribution

$$f_\alpha^{eq} = \omega_\alpha \rho_0 \exp\left(-\frac{U}{kT}\right)\left[1 + 3\frac{\mathbf{e}_\alpha \cdot \mathbf{u}}{c^2} + 9\frac{(\mathbf{e}_\alpha \cdot \mathbf{u})^2}{c^4} - \frac{3\mathbf{u}^2}{2c^2}\right], \qquad (7)$$

where $\omega_\alpha = \begin{cases} 4/9 & \alpha = 0 \\ 1/9 & \alpha = 1,2,3,4 \\ 1/36 & \alpha = 5,6,7,8 \end{cases}$.

Thus, the discrete density distribution satisfies the evolution equation

$$f_\alpha(\mathbf{r} + e_\alpha \delta_t, t + \delta_t) - f_\alpha(\mathbf{r}, t) = -\frac{1}{\tau_v}\left[f_\alpha(\mathbf{r}, t) - f_\alpha^{eq}(\mathbf{r}, t)\right] + \delta_t F_\alpha, \qquad (8)$$

where $\mathbf{r}$ is the position vector, δ_t is the time step defined as $\frac{\delta_x}{c}$, δ_x is the lattice constant, τ_ν is the dimensionless relaxation time, and $F_\alpha = \frac{\mathbf{G}\cdot(\mathbf{e}_\alpha - \mathbf{u})}{RT} f_\alpha^{eq}(\mathbf{r},t)$.

The macroscopic density and velocity can be calculated using

$$\rho = \sum_\alpha f_\alpha , \tag{9}$$

$$\rho\mathbf{u} = \sum_\alpha e_\alpha f_\alpha . \tag{10}$$

The dimensionless relaxation time, τ_ν, is a function of the fluid viscosity

$$\tau_\nu = 3\nu\frac{\delta_t}{\delta_x^2} + 0.5 , \tag{11}$$

where ν is the kinetic viscosity.

For electrokinetic flows in dilute electrolyte solutions, the external electrical force in Eq. (5) can be simplified to:

$$\mathbf{F}_E = \rho_e\mathbf{E} - \rho_e\nabla\Phi , \tag{12}$$

where Φ is the stream electrical potential caused by the ion movements in the solution based on the Earnst-Planck theory. Generally, the stream potential dominates the electro-viscosity effect in pressure driven flows, but its value is much less than the external potential and can be ignored in electrically driven flows. Therefore, the external force in the discrete Lattice Boltzmann equation (Eq. 8) should include the pressure and electric force

$$F_\alpha = \frac{(-\nabla P + \rho_e\mathbf{E} - \rho_e\nabla\Phi)\cdot(\mathbf{e}_\alpha - \mathbf{u})}{\rho RT} f_\alpha^{eq} . \tag{13}$$

Equations (6-13) can then be solved to analyze electro-kinetic flows using the LBM as long as the charge density distribution in the solution is known.

2.2 Lattice Poisson method for the electrical potential in the EDL

Electric double layer (EDL) theory [13] relates the electrostatic potential and the distribution of counter-ions and co-ions in the bulk solution by the Poisson equation as follows:

$$\nabla^2\psi = -\frac{\rho_e}{\varepsilon\varepsilon_0} , \tag{14}$$

where ψ is the electrical potential, ε is the dimensionless dielectric constant of the solution, ε_0 is the permittivity of a vacuum, and ρ_e is the net charge density. According to classical EDL theory, the equilibrium Boltzmann distribution equation can be used to describe the ionic number concentration. Therefore, the net charge density distribution can be expressed as the sum of all the ions in the solution:

$$\rho_e = \sum_i z_i e n_{i,\infty} \exp\left(-\frac{z_i e}{k_b T}\psi\right), \tag{15}$$

where the subscript i represents the ith species, n_∞ is the bulk ionic number concentration, z is the valence of the ions (including the sign), e is the absolute value of one proton charge, k_b is the Boltzmann constant, and T is the absolute temperature.

Substituting Eq. (15) into Eq. (14) yields the nonlinear Poisson equation for the electrical potential in the dilute electrolyte solution:

$$\nabla^2\psi = -\frac{1}{\varepsilon\varepsilon_0}\sum_i z_i e n_{i,\infty}\exp\left(-\frac{z_i e}{k_b T}\psi\right). \quad (16)$$

Eq. (16) can be solved using 1D or 2D linearized simplifications [16-18], iteration [14, 15] or multigrid methods [21,26]. Hirabayashi et al [32,33] ever developed a lattice BGK model for the Poisson equation where, however, the source term was linear or a fluctuation near zero. The model was hardly used directly to solve a nonlinear Poisson-Boltzmann equation. Here the lattice Poisson method (LPM), derived from the LBM [29,30], was used to solve Eq. (16).

The solution of Eq. (16) can be regarded as the steady solution of:

$$\frac{\partial\psi}{\partial t} = \nabla^2\psi + g_{rhs}(\mathbf{r},\psi,t), \quad (17)$$

where $g_{rhs} = \frac{1}{\varepsilon\varepsilon_0}\sum_i z_i e n_{i,\infty}\exp\left(-\frac{z_i e}{k_b T}\psi\right)$ represents the negative right hand side (RHS) term of the original Poisson equation.

The evolution equation for the electrical potential on the two-dimensional discrete lattices can then be written as

$$g_\alpha(\mathbf{r}+e_\alpha\delta_{t,g}, t+\delta_{t,g}) - g_\alpha(\mathbf{r},t) = -\frac{1}{\tau_g}\left[g_\alpha(\mathbf{r},t) - g_\alpha^{eq}(\mathbf{r},t)\right] + (1-\frac{0.5}{\tau_g})\delta_{t,g}\omega_\alpha g_{rhs}, \quad (18)$$

with the equilibrium distribution of g

$$g_\alpha^{eq} = \varpi_\alpha\psi \text{, with } \varpi_\alpha = \begin{cases} 0 & \alpha = 0 \\ 1/6 & \alpha = 1,2,3,4 \\ 1/12 & \alpha = 5,6,7,8 \end{cases} \quad (19)$$

The time step in Eq. (18) is

$$\delta_{t,g} = \frac{\delta_x}{c'}, \quad (20)$$

where c' is a *pseudo* sound speed in the potential field. In fact it can be artificial to vary the time step. The dimensionless relaxation time for Eq. (18) is

$$\tau_g = \frac{3\chi\delta_{t,g}}{2\delta_x^2} + 0.5, \quad (21)$$

where χ, which is equal to unity in the simulations, is defined as the potential diffusivity.

The evolution equations (18-21) can be proved consistent with the macroscopic Poisson equation (17). After evolving on the discrete lattices, the macroscopic electrical potential can be calculated using

$$\psi = \sum_\alpha (g_\alpha + 0.5\delta_{t,g} g_{rhs}\omega_\alpha). \quad (22)$$

Though the electrical potential evolution equations are in an un-steady form, only the steady state result is realistic, because the electromagnetic susceptibility has not been considered. The LPM has most of the advantages of the Lattice Boltzmann method and is suitable for complex flows and parallel computing. Although this paper only presents 2D cases, the algorithm is easy to extend to a 3D case.

2.3 Boundary conditions

The boundary conditions for LBM are very simple. The bounce-back model was used to model the fluid-solid interaction on the wall surfaces. Periodic conditions were implemented at the inlet and outlet.

The LPM for the electrical potential used the Dirichlet boundary condition on the wall surfaces and the Neumann condition at the inlet and outlet sections.

For the Dirichlet boundary, the unknown distribution functions were calculated from the local equilibrium distribution with the source, g_{rhs} [34]. For example, for the upper wall, g_4, g_7, and g_8 are unknown, but can be obtained from the equilibrium distribution of the local ψ_0:

$$\psi_0 = 3\psi_s - 3S_p - 1.5\delta_t \sum_\alpha \omega_\alpha g_{rhs}, \tag{23}$$

where S_p is the sum of known populations coming from the internal nodes and nearest wall nodes

$$S_p = g_0 + g_1 + g_2 + g_3 + g_5 + g_6, \tag{24}$$

and ψ_s is the boundary value. Thus the unknown distributions are

$$g_\alpha = \varpi_\alpha \psi_0, \tag{25}$$

The corner can be treated in a similar way, with five unknowns at the corner. The upper-right corner, for example, has the unknown populations g_3, g_4, g_6, g_7, and g_8. They also follow from Eq. (23) with

$$\psi_0 = \frac{12\psi_s - 6\delta_t \sum_\alpha \omega_\alpha g_{rhs} - 12S_p}{7}, \tag{26}$$

where

$$S_p = g_0 + g_1 + g_2 + g_5. \tag{27}$$

The inlet and outlet boundary for LPM was implemented the Neumann boundary conditions. At the outlet (the left section, for example), the relationship

$$\psi_0 = 3S_p + 1.5\delta_t \sum_\alpha (g_{rhs}\omega_\alpha c_{\alpha,x} / c), \tag{28}$$

with

$$S_p = g_1 + g_5 + g_8, \tag{29}$$

can be applied to determine the unknown populations g_3, g_6 and g_7.

3. Results and Discussion

The LPBM was used to simulate the EOF in a 2D microchannel as shown in Figure 1. The charges on the channel walls are either homogeneous or heterogeneous, so that the zeta potential distributions on the upper and lower walls are $\zeta_1(x)$ and $\zeta_2(x)$. The channel is H wide and L long. The electrolyte solution in the channel is driven by an electrical field, a pressure field or both.

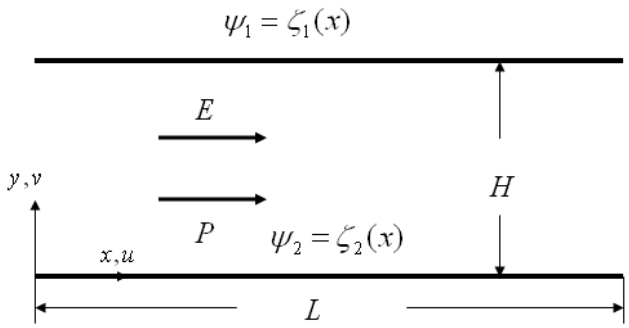

Figure 1 Boundary conditions for the electro-osmotic flow in a microchannel

This section first presents a validation of the method by comparison to an analytical solution and then uses the method to analyze electrical driven osmotic flow, the electro-viscosity effect, and electrical mixing enhancement.

3.1 Benchmark

For a 1:1 electrolyte solution flowing in a microchannel with periodic inlet/outlet boundaries and homogeneous walls, the Poisson-Boltzmann equation Eq. (16) can be simplified into the one-dimensional form:

$$\frac{d^2\psi}{dy^2} = \frac{2n_\infty ze}{\varepsilon\varepsilon_0}\sinh\left(\frac{ze}{kT}\psi\right). \tag{30}$$

If $ze\psi / kT$ is small, $\sinh(ze\psi / kT) \approx ze\psi / kT$. Eq. (30) can be linearized as:

$$\frac{d^2\psi}{dy^2} = \frac{2n_\infty z^2e^2}{\varepsilon\varepsilon_0 kT}\psi = \kappa^2\psi, \tag{31}$$

where $\kappa = \sqrt{\frac{2n_\infty z^2e^2}{\varepsilon\varepsilon_0 kT}}$ is defined as the reciprocal of the Debye length in Debye-Huckel theory. The linear one-dimensional ordinary differential equation in Eq. (31) has a simple analytical solution for a specified set of boundary conditions.

Figure 2 compares the LPM results for the non-linear Poisson-Boltzmann equation (Eq. 16) and the analytical solutions of the linearized equation (Eq. 31), together with numerical solution using the multigrid method. The parameters are an the ionic molar concentration $c_\infty = 10^{-4}M$, $n_\infty = c_\infty N_A$ where N_A is the Avogadro's number, $z = 1$, the dielectric constant of the solution $\varepsilon\varepsilon_0 = 6.95\times10^{-10}C^2 / J\cdot m$, the temperature $T = 273K$, and $\psi_1 = \psi_2 = \psi_s$ with ψ_s as a constant.

In general, the linearization is accurate when ψ is small. Figure 2 shows that the LPM results agree perfectly with multigrid solutions at all zeta potentials and with the analytical solution of the linearized equation when the absolute value of the surface zeta potential ζ is small, less than about 30 mV. This validates the accuracy of the LPM. When the absolute value of zeta potential is large (> 30 mV), the LPM numerical results depart from the linearized analytical solutions as expected [35,16].

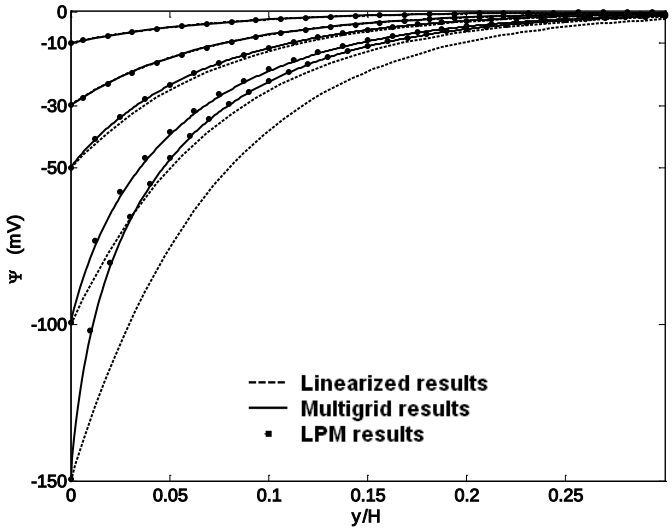

Figure 2 LPM results compared with the linearization results and the multigrid results for various surface zeta potentials (-10 mV, -30 mV, -50 mV, -100 mV and -150 mV).

3.2 Applications

After the LPM was validated, the LPBM was used to simulate electro-osmotic flows in microchannels. The LPM was first used to calculate the potential distribution in the domain to calculate the force per unit mass on the fluid. This force was then used in the LBM to calculate the EOF in microchannels.

3.2.1 Electrically driven osmotic flow

The First example considers a flow that is driven by only the electrical field in a homogeneous microchannel. The inlet and outlet boundaries are periodic. The channel is 0.8 μm wide and the ionic molar concentration far from the wall surface is 10^{-4} M for the results shown in Figure 3. As has been previously observed in qualitative results both experimentally [15] and numerically [36,37], the velocity in the electrically driven osmotic flow is nearly proportional to the external electrical field strength, as well as the surface zeta potential in a homogeneous channel. Recently, these results were also observed in MD simulations in nanochannel flows [38,39].

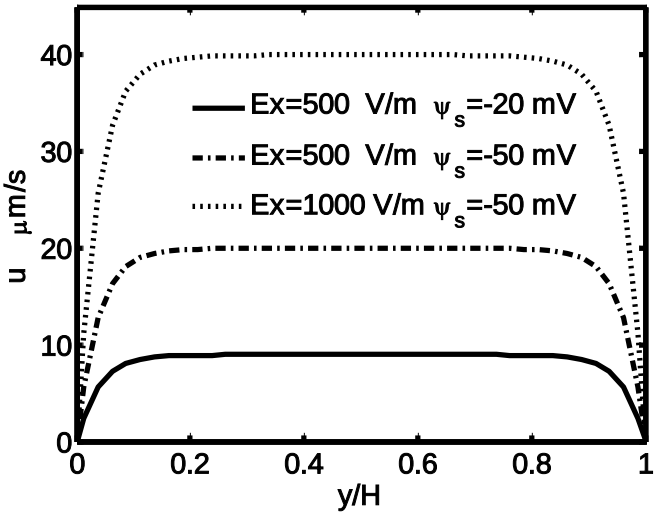

Figure 3 Velocity profiles for various external electrical fields and different surface zeta potentials. The solid line: E =5×10^2 V/m, ψ_s =-20 mV; the dot-line: E =5×10^2 V/m, ψ_s =-50 mV; the dashed-line: E =1×10^3 V/m, ψ_s =-50 mV.

The velocity profiles for the various ionic concentrations far from the walls are shown in Figure 4 for a channel width is 0.4 μm, the external electric field strength E =5×10^2 V/m, and the surface zeta potential ψ_s =-50 mV for both walls. The fluid properties are set as those of water at the standard state which are the dielectric constant $\varepsilon\varepsilon_0 = 6.95\times10^{-10} C^2/J\cdot m$, the density ρ =1.0×10^3 kg/m^3 and the viscosity μ =0.89 Pa s. The results show an optimal ionic concentration that maximizes average velocity. As the ionic molar concentration decreases from a high value (2×10^{-2}), the EDL thickness increases so that although the force is slightly reduced, the electrical force domain increases and thus the average velocity increases. There exists a concentration at which the effect of the electrical force can dominate across the entire channel and make the velocity reach maximum (10^{-4}~10^{-3} M for current simulations). As the ionic concentration decreasing (such as from 10^{-4} to 10^{-6}), the force reduction becomes the most important factor and the average velocity decrease. The lower ionic concentrations also result in a more parabolic-like velocity profile.

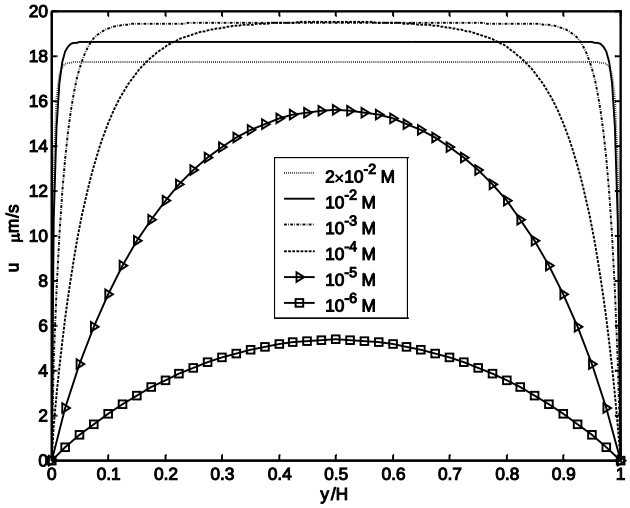

Figure 4 Velocity profiles for various ionic molar concentrations for electrically driven flow. The dotted line: c_∞ =2×10^{-2} M; the solid line: c_∞ =10^{-2} M; the dash-dot line: c_∞ =10^{-3} M; the dashed line: c_∞ =10^{-4} M; the triangle-line: c_∞ =10^{-5} M; the square-line: c_∞ =10^{-6} M.

Figure 5 shows the velocity profiles for various channel widths for c_∞ =10^{-4} M, E =5×10^2 V/m, and ψ_s =-50 mV. The channel width varies from 0.1 μm to 1 μm. The average velocity shows good monotonicity with the channel width. For channel widths larger than double size of the EDL thickness, the maximum velocity seldom changes with the channel width. However, for channels widths less than double size of the EDL thickness, a smaller channel width leads to a smaller velocity.

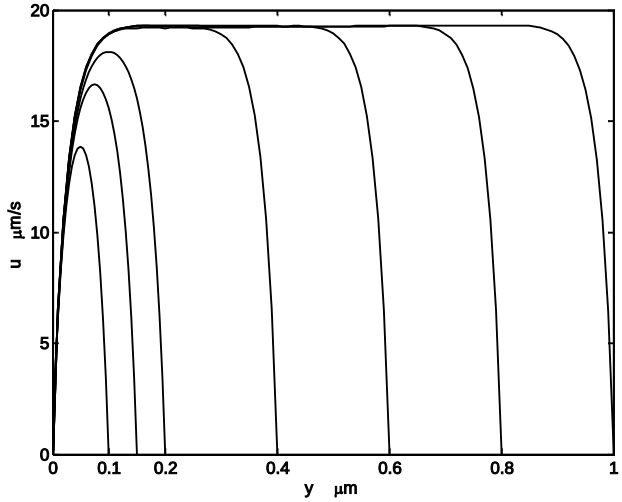

Figure 5 Velocity profiles for different channel widths.

3.2.2 Electro-viscosity effect

When an electrolyte solution flows in a microchannel driven only by the pressure gradient, the charged wall surface will increase the resistance, which is defined as the electro-viscosity effect. This effect has been proven experimentally [11]. New dynamic models based on the Navier-Stokes equations have been built to model this effect [12,40,41]. Tian et al. [36] simulated the electro-viscosity effect using the LBM, but they did not find any significant difference between the results with and without the EDL. The following example investigates this effect using the LPBM.

For 2D electrokinetic steady-state flow in microchannels, the streaming potential, Φ, in Eq. (12) can be defined by the constraint of current continuity [17,37]:

$$\Phi = -L\frac{\int_0^H u(x,y)\rho_e(x,y)dy}{(\lambda_b + \lambda_s\kappa)H}, \qquad (36)$$

where λ_b is the electrical conductivity of the bulk fluid and λ_s is the surface conductance. In the present simulations, λ_b is 1.42×10^{-3} S/m and λ_s is 1.64×10^{-9} S.

Velocity profile for flow in a homogeneous channel are show in Figure 6 for a channel having a width of 0.4 μm, $c_\infty = 10^{-4}$ M, $dP/dx = 1\times10^6$ Pa/m, and surface zeta potentials, ψ_s, from 0 mV to -70 mV. When $|\psi_s|$ is very small (1 mV), the velocity profile is the same as the non-EDL channel flow profile. When $|\psi_s|$ is larger than 10 mV, the electro-viscosity effect becomes significant and the effect increases with the increasing $|\psi_s|$. Unlike the regular viscosity effect, the electro-viscosity effect mainly affects the velocity distribution near the wall so that the viscosity profiles near the walls are no longer parabolic.

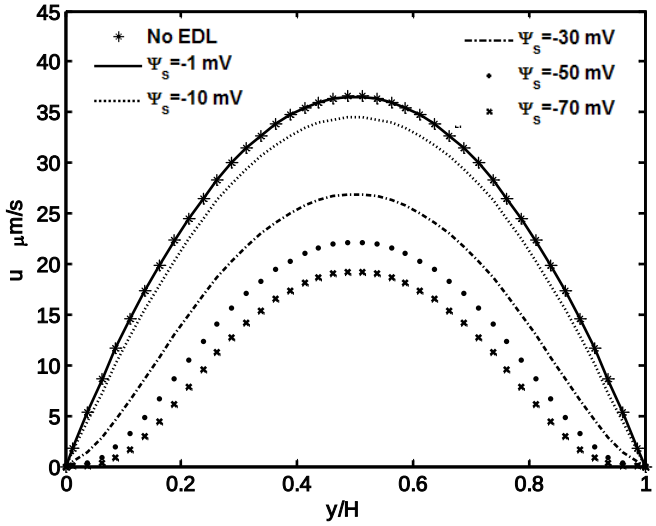

Figure 6 Velocity profiles for various surface zeta potentials in a homogeneous channel with pressure driven flow. The asterisk (*): ψ_s =0 mV; the solid line: ψ_s =-1 mV; the dashed line: ψ_s =-10 mV; the cross sign: ψ_s =-30 mV; the diamond sign: ψ_s =-50 mV; the triangle sign: ψ_s =-70 mV.

Figure 7 shows the velocity profiles plotted as a function of the ionic concentrations for ψ_s =-50 mV. The ionic concentrations vary from 10^{-4} M to 10^{-6} M. When its value drops from 10^{-4} to 10^{-5}, the velocity drops (from the solid line to the dashed line) in the bulk flow region. As the value drops on from 10^{-5} to 10^{-6}, the velocity profile rises up totally (see the dash-dot line). It can be foreseen that the velocity profile will approach the non-EDL case (the dot line) with the ionic concentration drops on. The figure indicates that the electro-viscosity varies non-monotonically with the ionic concentration. The reason is quite similar with the electrically driven cases. There exists an ionic concentration value

yielding the largest electro-viscosity effect. Additionally, a lower ionic concentration leads to a more parabolic velocity profile.

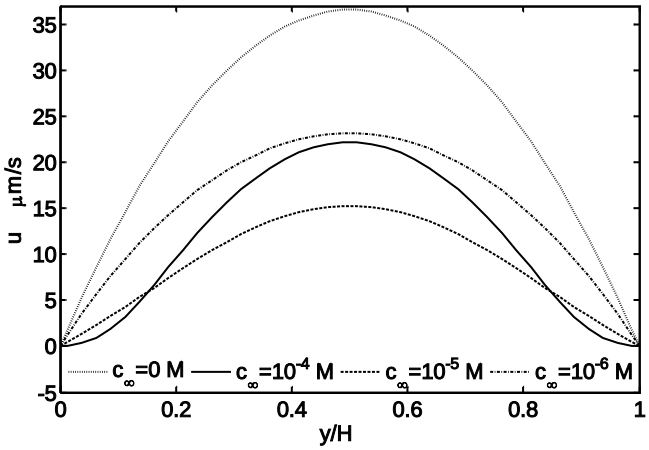

Figure 7 Velocity profiles for various ionic concentrations in a homogeneous channel. The dotted-line: c_∞ =0 M; the solid line: c_∞ =10^{-4} M; the dashed line: c_∞ =10^{-5} M; the dashed-dot line: c_∞ =10^{-6} M.

The second example illustrates the electro-viscosity effect in heterogeneous channels. Four cases were considered:

Case 1: $\psi_1 = \psi_s,\ x \in (0, L)$; $\psi_2 = \psi_s,\ x \in (0, L)$. (Homogeneous)

Case 2: $\psi_1 = \psi_s,\ x \in (0, L)$; $\psi_2 = -\psi_s,\ x \in (0, L)$. (Oppositely charged)

Case 3: $\psi_1 = \psi_s,\ x \in (0, L/4) \cup (L/2, 3L/4)$; $\psi_1 = -\psi_s,\ x \in (L/4, L/2) \cup (3L/4, L)$;

$\psi_2 = \psi_s,\ x \in (0, L/4) \cup (L/2, 3L/4)$; $\psi_2 = -\psi_s,\ x \in (L/4, L/2) \cup (3L/4, L)$.

Case 4: $\psi_1 = \psi_s,\ x \in (0, L/4) \cup (L/2, 3L/4)$; $\psi_1 = -\psi_s,\ x \in (L/4, L/2) \cup (3L/4, L)$;

$\psi_2 = -\psi_s,\ x \in (0, L/4) \cup (L/2, 3L/4)$; $\psi_2 = \psi_s,\ x \in (L/4, L/2) \cup (3L/4, L)$.

Figure 8 compares the velocity profiles of channel middle sections (A-A section in Fig. 1) for H =0.4 μm, c_∞ =10^{-4} M, dP/dx =1×10^6 Pa/m, and ψ_s =-50 mV. All four cases have significant electro-viscosity effects when compared with the non-EDL case. The resistance of the homogeneous one (case 1) is the largest, while that of the oppositely charged case is the smallest. The velocity profiles for cases 3 and 4 are almost the same and fall between case 1 and 2.

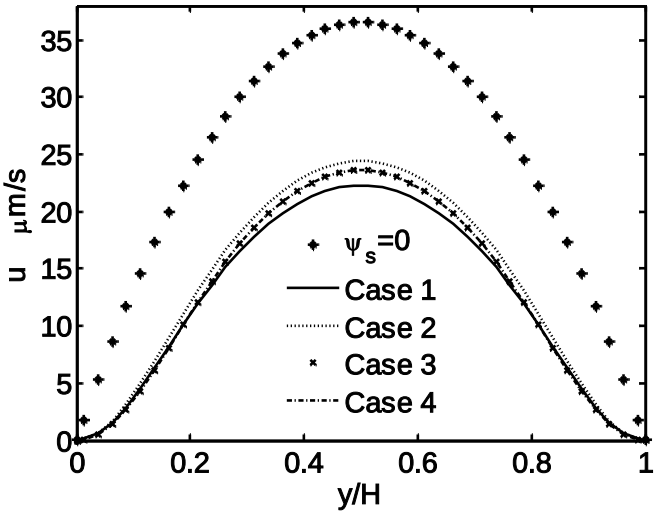

Figure 8 Velocity profiles for various surface zeta potential distributions in heterogeneous channels

3.2.3 Electrical mixing enhancement

The final example illustrates a flow driven by both the electrical force and the pressure gradient in microchannels. These conditions are usually used for mixing enhancement [9,10]. The conditions are the same as for case 3 and 4 in section 3.2.2 with an additional external electrical field of $E=5\times10^2$ V/m. The calculated velocity contours are shown in Figure 9. The electrical force causes vortices to appear near the surface that act as small stirrers in the channel. If two kinds of fluids or a suspension flows in the channels, the vortices will enhance the mixing. The mixing strength can be easily controlled by changing the electrical field strength or the zeta potentials. The streamlines along the channel mid-line show qualitatively that case 4 has better mixing enhancement efficiency than case 3 due to its much larger y-velocities. Similar results can be found in reference [42].

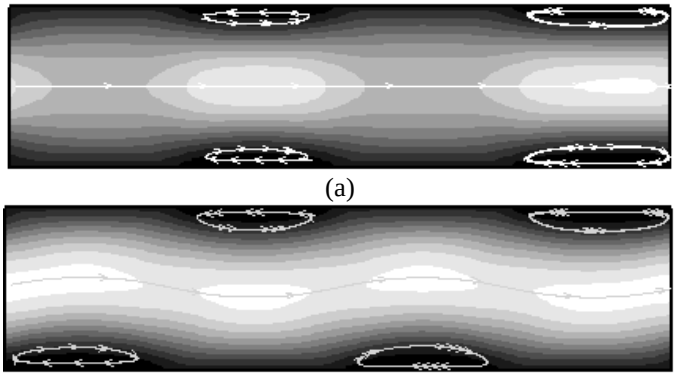

(a)

(b)

Figure 9 Velocity contours for different heterogeneous zeta potential distributions in electro-pressure driven flows. (a) case 3 zeta potential arrangement; (b) case 4 zeta potential arrangement.

The vortices generation dissipates the kinetic energy of the fluid. Therefore, the energy dissipation is also a very important factor when selecting a scheme for enhancing mixings. The velocity profiles at $x=L/2$ (A-A section in Fig. 1) for the two cases are compared in Figure.10. The figure shows that the zeta potential arrangement in case 4 has less energy dissipation than that in case 3. Thus, considering both the mixing effect and the energy dissipation, the zeta potential arrangement in case 4 is a better scheme for electrically driven mixing enhancement.

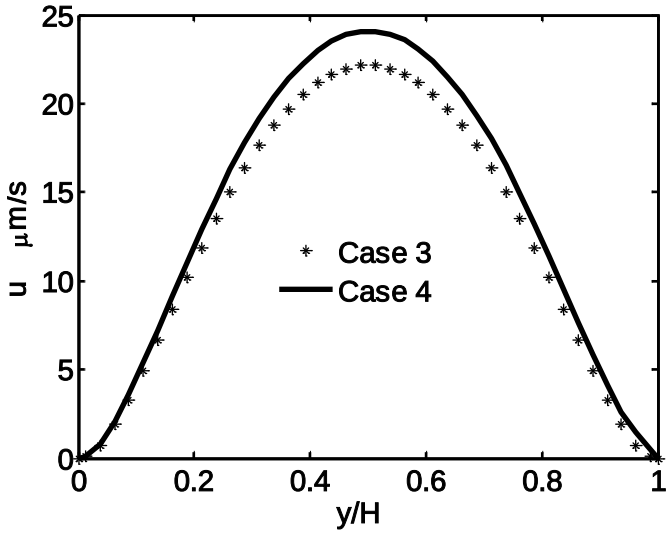

Figure 10 Velocity profiles at $x=L/2$ for electro pressure driven flow

4. Conclusions

The Lattice Poisson-Boltzmann method (LPBM), which combined a lattice Poisson method (LPM) solving the non-linear Poisson equation for electric potential and a lattice Boltzmann method (LBM) solving the Navier-Stokes equations

for fluid, was used to simulate the electro-osmotic flows in microchannels. For electrically driven osmotic flows, the flow velocity is nearly proportional to the external electrical field strength and the surface zeta potential value for flows in homogeneous channels. However the flow velocity changes with the ionic concentration and the channel width are more complex. For a given set of conditions, the flows have an optimal ionic concentration or channel width that maximizes the average velocity. For pressure-driven flows, the electro-viscosity effect increases monotonically with the surface zeta potential, but reaches a maximum and then decreases with increasing ionic concentration. The zeta potential arrangement has little effect on the electro-viscosity for heterogeneous channels. Flows driven by both an electrical force and a pressure gradient can be used to enhance mixing in the fluid. The mixing enhancement was analyzed by comparing the flow fields in channels with different zeta potential arrangements, including the mixing enhancement effects and the energy dissipation. Since the electro-osmotic flows in microchannels have many promising applications in microsystems, the analyzed methods and simulations presented here provide valuable information for the design and optimization of MEMS/NEMS.

Acknowledgements

The present work was supported by the National Natural Science Foundation of China (Grant No. 59995550-2). M.W. would like to thank Prof. Chen SY and Prof. Zhao TS for encouragement and helpful discussions. The authors also thank Dr Guo ZL and Dr Tian FZ for discussions.

References

[1] Wong PK, Wang JT, Deval JH, and Ho CM. 2004. Electrokinetic in Micro Devices for Biotechnology Applications. *IEEE/ASME Transactions on Mechatronics*, **9**: 366-376.

[2] Stone HA, Stroock AD and Ajdari A. 2004. Engineering Flows in Small Devices: Microfluidics Toward a Lab-on-a-Chip. *Annu. Rev. Fluid Mech*. **36**: 381-411.

[3] Lowen H. 2004. The marriage of electrostatics and hydrodanamics: simulating the dynamics of charged colloids. *Journal of Physics: Condensed Matter*. **16**: V7-V9.

[4] Reyes D, Iossifidis D, Auroux P, and Manz A. 2002. Micro Total Analysis Systems. 1. Introduction, Theory, and Technology. *Anal. Chem*. **74**: 2623-2636.

[5] Brask A, Goranovi´c G, Jensen MJ, and Bruus H. 2005. A novel electro-osmotic pump design for nonconducting liquids: theoretical analysis of flow rate–pressure characteristics and stability. *J. Micromech. Microeng.* **15:** 883–891.

[6] Pu QS, Liu SR. 2004. Microfabricated electroosmotic pump for capillary-based sequential injection analysis**.** *Anal. Chim. Acta.* **511:** 105-112.

[7] Bazant MZ, Squires TM. 2004. Induced-charge electrokinetic phenomena: Theory and microfluidic applications. *Phys. Rev. Lett.* **92**: 066101.

[8] Squires TM, Bazant MZ. 2004. Induced-charge electro-osmosis. *J. Fluid Mech*. **509**: 217-252.

[9] Nguyen NT, and Wu ZG. 2005. Micromixers—a review. *J. Microeng. Micromech*. **15**: R1-R16.

[10] Shin SM, Kang IS, and Cho YK. 2005. Mixing enhancement by using electrokinetic instability under time-periodic electric field. *J. Micromech. Microeng*. **15:** 455–462.

[11] Ren L, Li D and Qu W. 2001. Electro-Viscous Effects on Liquid Flow in Microchannels. *J. Colloid and Interface Science*. **233**: 12-22.

[12] Ren CL, Li D. 2005 Improved understanding of the effect of electrical double layer on pressure-driven flow in microchannels. *Analytica Chimica Acta.* **531** (1): 15-23.

[13] Masliyah, JH. *Electrokinetic Transport Phenomena* (Alberta Oil Sands Technology and Research Authority. Alberta, Canada, 1994)

[14] Li D. 2001. Electro-viscous effects on pressure-driven liquid flow in microchannels. *Journal of Colloids and Surfaces*. **195**: 35-57.

[15] Sinton D, Li D. 2003. Electroosmotic velocity profiles in microchannels. *Journal of Colloids and Surfaces A*. **222:** 273-283.

[16] Li B, Kwok DY. 2003. Lattice Boltzmann model of microfluidics with high Reynolds numbers in the presence of external. *Langmuir*. **19:** 3041-3048.

[17] Li B, Kwok DY. 2004. Electrokinetic microfluidic phenomena by a lattice Boltzmann model using a modified Poisson-Boltzmann equation with an excluded volume effect. *J. Chem. Phys*. **120**: 947-953.

[18] Tian FZ, Li BM, and Kwok DY. 2005. Tradeoff between mixing and transport for electroosmotic flow in heterogeneous microchannels with nonuniform surface potentials. *Langmuir*. **21** (3): 1126-1131.

[19] Qiao R, Aluru NR. 2003. Ion concentrations and velocity profiles in nanochannel electroosmotic flows. *J. Chem. Phys*. **118**: 4692-4701.

[20] Darguji H, Yang PD, and Majumdar A. 2004. Ion Transport in Nanofluidic Channels. *Nano Letters*. **4**: 137-142.

[21] Melchionna S, and Succi S. 2004. Electrorheology in nanopores via lattice Boltzmann simulation. *Journal of Chemical Physics*. **120**: 4492-4497.
[22] Warren PB. 1997. Electroviscous transport problems via lattice-Boltzmann. *International Journal of Modern Physics C*. **8** (4): 889-898.
[23] He XY, and Li N. 2000. Lattice Boltzmann simulation of electrochemical systems. *Computer Physics Communications*. **129**: 158-166.
[24] Horbach J, and Frenkel D. 2001. Lattice-Boltzmann method for the simulation of transport phenomena in charged colloids. *Physical Review E*. **64**: 061507.
[25] Guo ZL, Zhao TS, and Shi Y. 2005. A lattice Boltzmann algorithm for electro-osmotic flows in microfluidic devices. *Journal of Chemical Physics*. (In Press)
[26] Wu J, Srinivasan V, Xu J, and Wang C.Y. 2002. Newton-Krylov-Multigrid Algorithms for Battery Simulation. *Journal of the electrochemical society*, **149**(10): A1342-A1348.
[27] Frenkel D, and Ernst M. H. 1989. Simulation of diffusion in a two-dimensional lattice-gas cellular automaton: A test of mode-coupling theory. *Phys. Rev. Lett*. **63**: 2165–2168.
[28] Chen S, Doolen GD. 1998. Lattice Boltzmann method for fluid flows. *Annu. Rev. Fluid Mech.* **30**: 329-364.
[29] He XY, Luo LS. 1997. Theory of the lattice Boltzmann method: From the Boltzmann equation to the lattice Boltzmann equation. *Phys. Rev. E.* **56** (6): 6811-6817.
[30] He XY, Chen S, and Doolen G. 1998. A novel thermal model for the lattice Boltzmann method in incompressible limit. *J. Comput. Phys*, **42**(146): 282-300.
[31] Guo ZL, Zheng CG, Shi BC. 2002. Discrete lattice effects on the forcing term in the lattice Boltzmann method *Phys. Rev. E* **65(4)**: 046308
[32] Hirabayashi M, Chen Y, Ohashi H 2001. The lattice BGK model for the Poisson equation, *JSME International Journal Series B* **44 (1):** 45-52.
[33] Hirabayashi M, Chen Y, Ohashi H. 2000. The lattice BGK solution of the QKPZ equation: Universlity and Scaling in Fluid Invasion of Porous Media. *Transactions of JSCES*, Paper-20000004
[34] D'Orazio A., Succi S. 2004. Simulating two-dimensional thermal channel flows by means of a lattice Boltzmann method with new boundary conditions. *Future Generation Computer Systems*. **20**(6): 935-944.
[35] Flatt RJ and Bowen P. 2003. Electrostatic repulsion between particles in cement suspensions: Domain of validity of linearized Poissn-Boltzmann equation for nonideal electrolytes. Cement and concrete Research. **33**: 781-791
[36] Tian FZ, Li BM, and Kwok DY. 2004. Lattice Boltzmann Simulation of Microfluidics with Non-uniform zeta Potentials: Requirements of Flow Rate and Current Continuities. In: *International Conference on MEMS, NANO and Smart Systems (ICMENS) of 2004*. Banff, Alberta, Canada. pp.644-649.
[37] Tian FZ, Li BM, and Kwok DY. 2004. Lattice Boltzmann Simulation of Electroosmotic Flows in Micro- and Nanochannels In: *International Conference on MEMS, NANO and Smart Systems (ICMENS) of 2004*. Banff, Alberta, Canada. pp. 294-299.
[38] Cui ST and Cochran HD. 2004. Electroosmotic Flow in Nanoscale Parallel-plate Channels: Molecular Simulation Study and Comparison with Classical Poisson–Boltzmann Theory. *Molecular Simulation*, **30(5)**: 259–266
[39] Zhu W, Singer SJ, Zheng Z, et al. 2005. Electro-osmotic flow of a model electro-lyte. *Phys. Rev. E* **71(4)**: 041501
[40] Ren CL, Li D. 2004. Electroviscous effects on pressure-driven flow of dilute electrolyte solutions in small microchannels. *Journal of Colloid and Interface Science*. **274** (1): 319-330.
[41] Lee JSH, Ren CL, and Li D. 2005. Effects of surface heterogeneity on flow circulation in electroosmotic flow in microchannels. *Analytica Chimica Acta*. **530**: 273-282
[42] Erickson D, Li D. 2002. Influence of Surface Heterogeneity on Electrokinetically Driven Microfluidic Mixing. *Langmuir*. **18**(5): 1883-1892